Nonlinear modes in rotating double well potential with parity–time symmetry*

Pang Wei(庞 玮)[a], Fu Shen-He(付神贺)[b], Wu Jian-Xiong(吴剑雄)[c]
Li Yong-Yao(黎永耀)[d], and Mai Zhi-Jie(麦志杰)[d]†

[a] Department of Experiment Teaching, Guangdong University of Technology, Guangzhou 510006, China
[b] State Key Laboratory of Optoelectronic Materials and Technologies, Sun Yat-Sen University, Guangzhou 510275, China
[c] Department of Electrical and Computer Engineering, University of Toronto, Toronto, M5S3G4, Canada
[d] Department of Applied Physics, South China Agricultural University, Guangzhou 510642, China

(Received 25 November 2013; revised manuscript received 6 January 2014; published online 10 August 2014)

We investigate the nonlinear modes in a rotating double well potential with $\mathcal{PT}$ symmetry. Focus on the existence and stability of the nonlinear PT modes in this system, we found that five types of PT modes can stably exist by given certain parameter settings. The multistable area between these modes are studied numerically and the bistable and tristable areas are delimited. With different input trial wavefunctions, five types of solitary wave modes are identified. We found that the rotating of the potential can significantly affect the power flow of the fundamental harmonic mode, whose effect is absent for the other modes.

Keywords: parity–time mode, rotating double well potential, parity–time symmetric, stability diagram

PACS: 42.65.Tg, 42.65.Jx, 42.65.Wi **DOI:** 10.1088/1674-1056/23/10/104214

1. Introduction

Parity–time ($\mathcal{PT}$) symmetry as a concept originated from the field theory[1] and be revived in the late 1990s mainly by Bender and Boettcher[2] who found that, instead of the conventional requirement of the Hamiltonian to be Hermitian, a non-Hermitian Hamiltonian but with certain kinds of parity–time symmetry can also produce a real energy spectrum and preserves the unitarity of the time evolution. A necessary condition for a Hamiltonian with complex potential $V(x)$ to have $\mathcal{PT}$ symmetry can be reduced to the requirement that $V(x) = V^*(-x)$,[2,3] which implies that the real part of the potential must be an even function of position x and the imaginary part must be an odd function of x. Such systems can be realized in various scenarios, as recently experimentally achieved in optics by passive or active $\mathcal{PT}$-dimers[4,5] and periodic lattice[6] and very recently by coupled electronic oscillators.[7] Other suggestions include atomic settings,[8] electrical analog systems,[9] microwave billiards[10] or even $\mathcal{PT}$-symmetric oligomers as blocks to construct complex $\mathcal{PT}$-symmetric lattices.[11,12]

As an alternative to the Hermitian quantum mechanics, $\mathcal{PT}$ symmetric systems drew lots of interests in recent years, theoretically and experimentally.[1,13] Among them, special concerns have been shed on the nonlinear waves (i.e., solitary waves) and modes in a system with $\mathcal{PT}$ symmetry. In a conventional system with dissipation, the solitary waves can exist only as isolated solutions for some discrete parameters, as in the Ginzberg–Landau equations,[14] however, in a system with $\mathcal{PT}$ symmetry, despite the dissipative gain and loss, all the real energy levels guarantee that all the linear modes still exhibit as regular waves, which leads to the existence of continuous families of solitons in the system. This novelty feature has inspired the study of solitons in diverse optical potentials with $\mathcal{PT}$ symmetric gain and loss, including linear lattices,[15–17] nonlinear lattices,[18,19] mixed linear–nonlinear lattices,[20–25] discrete lattices,[26] continuous families of solitons are found to exist in these systems. Existence and stability features of the solitons in $\mathcal{PT}$ symmetric systems are also investigated.[27]

Except for all kinds of linear and/or nonlinear lattices, another well-known tool to create various dynamical states is provided by rotating potentials. A stirring of media with intrinsic nonlinearity can exhibit lots of interesting effects, especially in Bose–Einstein condensates (BEC), namely the formation of vortex lattices,[28] giant vortices,[29] quasisolitons.[30] Furthermore, by implementing a broad laser beam transmitted through a revolving sieve,[31] or using twisted photonic-crystal fibers,[32] a rotating lattice can be created as well. Ground-state soliton, vortex soliton,[33] gap soliton,[34] and two-dimensional (2D) solitons[35] are found to exist in such rotating lattices. Soliton modes and the symmetry breaking between them are also investigated.[36] A natural question is the existence and stability of nonlinear modes in a rotating lattice with $\mathcal{PT}$ symmetry. The simplest implementation of such settings is a revolving double-well potential, i.e., a one-dimensional (1D) double-well potential placed onto a rotating ring. In optics, it can be realized passively by a twisted hollow pipe waveguide, or actively by polarization pump waves[37] or electromagnetically induced transparency (EIT).[36,38–41] In

*Project supported by the National Natural Science Foundation of China (Grant Nos. 11104083 and 10934011).
†Corresponding author. E-mail: zhijiemai@gmail.com
© 2014 Chinese Physical Society and IOP Publishing Ltd

BEC, similar settings can be created by adding the potential to a ring-shaped trap[32] or equivalently by a rotating ring.[42] To introduce a $\mathcal{PT}$ symmetric potential to this revolving double-well potential, in optics this could be done via applied mutually balanced gain and loss to the refractive index profile,[4–6] while in terms of BEC a number of suggestions have been proposed, including injecting and removing atoms from the potential wells[7] or by three-level atoms.[43]

The aim of the present work is to investigate the basic types, existence, stability, and the symmetry breaking of the nonlinear modes trapped in a rotating double-well potential with $\mathcal{PT}$ symmetry. In Section 2 we formulate the model. Numerical results and discussion are presented in Section 3. The paper is concluded in Section 4.

2. Theoretical model

In this work, we consider a 1D double-well potential placed into a rotating ring, as shown in Fig. 1. In optics this setting can be realized by a hollow-pipe waveguide twisted with pitch $2\pi/\omega$ and the effective $\mathcal{PT}$ symmetric potential $V(\theta)$ can be written into the pipe as an azimuthal modulation of the refractive index; while in BEC, it can be created via a rotating ring, as mentioned above. In the thin helical shell limit, the radius of the helical shell can be regarded as a fixed value r_0, which we normalized to be $r_0 = 1$.

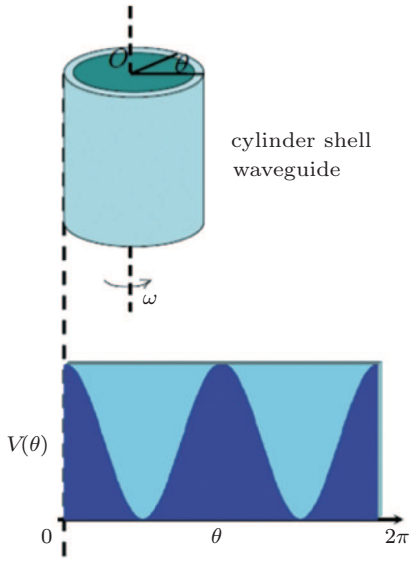


Fig. 1. (color online) The helical pipe waveguide with effective $\mathcal{PT}$ symmetric potential $V(x)$, twisted at rate ω. Only the real part of $V(\theta)$ is shown here.

The nonlinear wave modes in this setting can be described by a scaled nonlinear Schödinger equation in the corotating reference frame:[36,44,45]

$$\mathrm{i}\frac{\partial}{\partial z}\psi = \left[-\frac{1}{2}\frac{\partial^2}{\partial\theta^2} + \mathrm{i}\omega\frac{\partial}{\partial\theta} + a\cdot\cos(2\theta) + \mathrm{i}b\cdot\sin(2\theta) - \sigma|\psi|^2\right]\psi, \tag{1}$$

Here z is the propagation distance along the pipe and in the context of BEC z is replaced by time t.[46] ω is the angular rotating speed of the potentials, a and σ is the strength of the linear and nonlinear potentials respectively. $\sigma = +1$, and -1 refer to self-focusing (SF) and self-defocusing (SDF) nonlinearities and in this work we focus on the SDF case only, thus in the following context the sign of σ is fixed to be negative. b is the strength of the imaginary part of the $\mathcal{PT}$ symmetric potential and i is the imaginary unit. Noticed that the linear potential $a\cdot\cos(2\theta)$ could also be regarded as the even real part of a $\mathcal{PT}$ symmetric potential $V(\theta)$, with $\mathrm{i}b\cdot\sin(2\theta)$ as its odd imaginary part, i.e., $V(\theta) = a\cdot\cos(2\theta) + \mathrm{i}b\cdot\sin(2\theta)$, which fulfills the requirement of the $\mathcal{PT}$ complex potential mentioned above.

The stationary modes with real propagation constant $-\mu$ (in the context of BEC μ is the chemical potential) are sought for as $\psi(\theta,z) = \exp(-\mathrm{i}\mu z)\phi(\theta)$. Substituting this solution to Eq. (1) gives the equation obeying by the complex function $\phi(\theta)$:

$$\mu\phi = \left[-\frac{1}{2}\frac{\partial^2}{\partial\theta^2} + \mathrm{i}\omega\frac{\partial}{\partial\theta} + a\cdot\cos(2\theta) + \mathrm{i}b\cdot\sin(2\theta) - \sigma|\phi|^2\right]\phi. \tag{2}$$

The total power (norm in BEC) of the wave can be defined as:

$$P = \int_{-\pi}^{+\pi}|\phi(\theta)|^2\,\mathrm{d}\theta. \tag{3}$$

The periodic boundary conditions $V(\theta) = V(\theta + 2\pi)$ and the continuous requirement of the wave function $\phi(\theta) = \phi(\theta + 2\pi)$ leads to an azimuthal Bloch bands in this system,[43–45] which makes Eq. (1) and Eq. (2) invariant under boost transformation

$$\phi(\theta,z;\omega - N) = \phi(\theta,z;\omega)\exp\left[-\mathrm{i}N\theta + \mathrm{i}\left(\frac{1}{2}N^2 - N\omega\right)z\right]. \tag{4}$$

This invariance can restrict the rotating speed to the interval $0 \le \omega < 1$. Another observation of $\phi(\theta,z;\omega) = \phi^*(\theta,-z;-\omega)$ can further reduce this interval to $0 \le \omega \le 1/2$.[36]

In order to focus on the interplay of the rotating and the $\mathcal{PT}$ symmetric potential, here and after we fix the strength of the linear potential to be 1, namely $a = 1$. Other alternations, such as dropping the linear potential completely ($a = 0$) to make a pure imaginary potential with nonlinearity, will be considered elsewhere.

3. Numerical results and discussion

Equation (2) can be numerically solved by means of PC-SOM program.[47] With different input trial wave functions, five types of solitary wave modes can be identified in this

system, which is labeled as fundamental harmonic symmetry mode (FH), second harmonic symmetry mode (2H), fundamental harmonic symmetry breaking mode (FHB), second harmonic symmetry breaking mode (2HB), and anti-symmetry mode (AnS). The typical profile of these modes are shown in Figs. 2, 3, and 4. Here the fundamental and second harmonic modes (FH or 2H, respectively) are regarded by the dominant term in the Fourier decomposition of the stationary solution. The FHB and 2HB modes are identified by the shape of their density profiles.

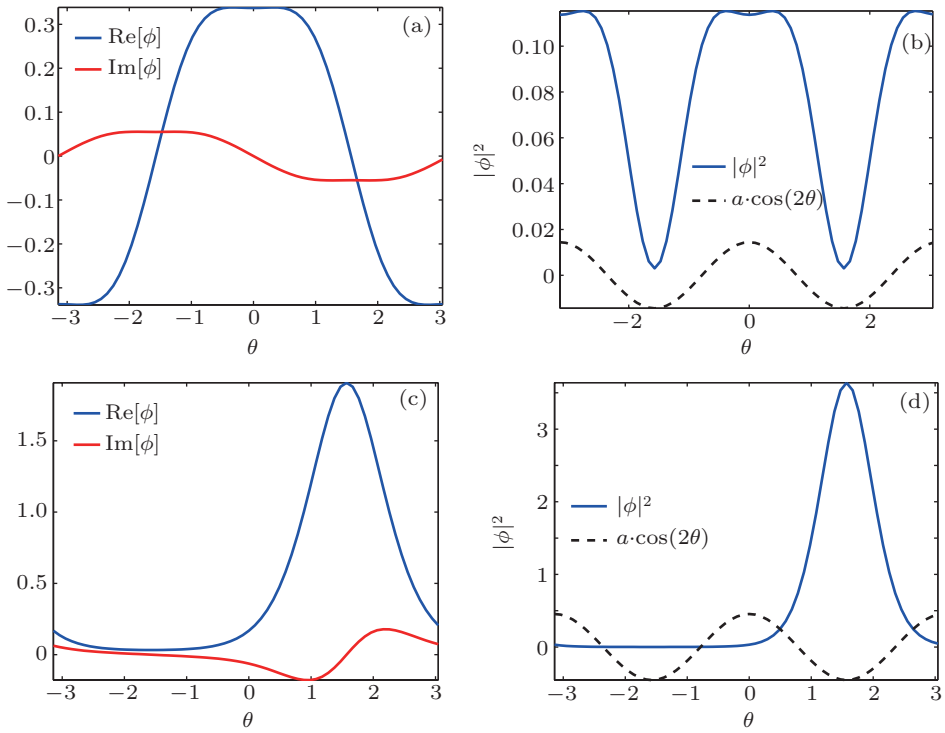


Fig. 2. (color online) Examples of stable FH and FHB modes with $b = 0.1$, $\omega = 0.2$. (a) and (c) Real and imaginary parts of the FH and FHB modes, respectively. (b) and (d) Intensity profiles of the same modes. For FH mode $P = 0.5$ and for FHB mode $P = 4.0$. The black dash curves in panels (b), (d), and similar panels in the following figures, depict the profile of the real part of the $\mathcal{PT}$ symmetric potential.

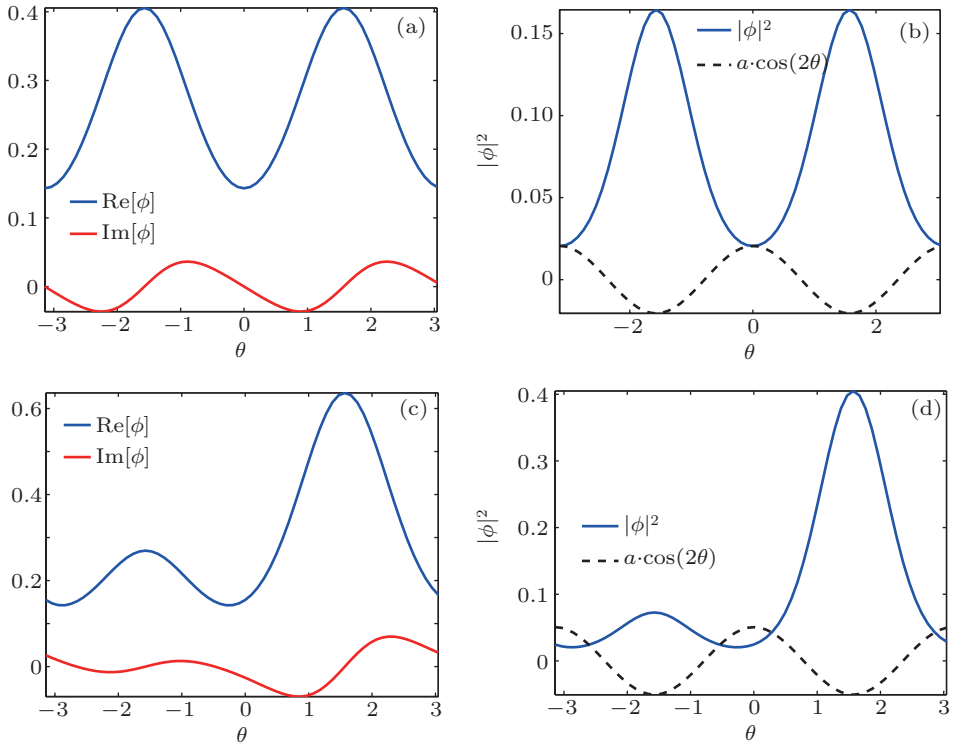


Fig. 3. (color online) Examples of stable 2H and 2HB modes with $b = 0.1$, $\omega = 0.2$. (a) and (c) Real and imaginary parts of the 2H and 2HB modes respectively. (b) and (d) Intensity profiles of the same modes. For 2H mode $P = 0.5$ and for 2HB mode $P = 0.7$.

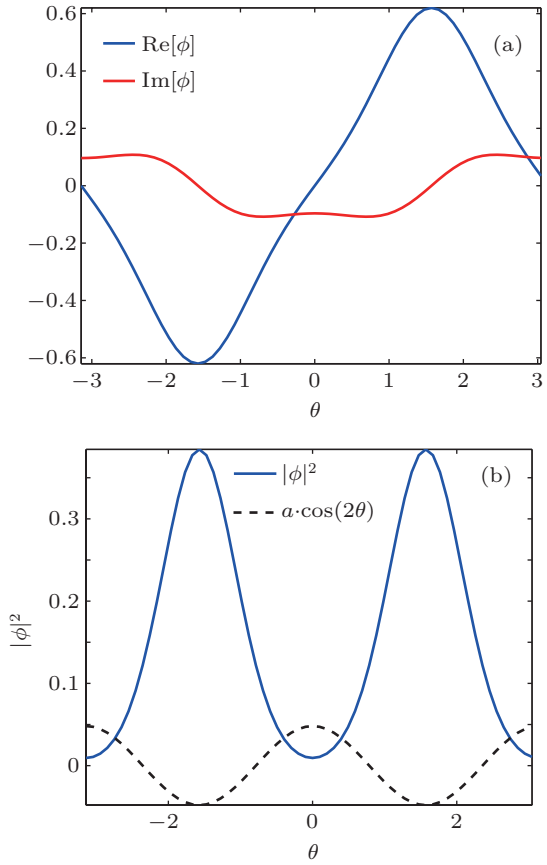


Fig. 4. (color online) Example of stable AnS mode with $b = 0.1$, $\omega = 0.2$ and $P = 1.0$. (a) Real and imaginary parts, of the AnS mode. (b) Intensity profiles of the same mode.

We can see from the density profiles Figs. 2(b), 2(d), 3(b), 3(d), and 4(b) that the maximum and minimum of the solitons are all located at the nodes of the real part of $V(\theta)$, i.e., $\theta = 0, \pm\pi/2, \pm\pi$. The FH mode has two peaks with equal strength, with the maximums located at $\theta = 0$ and π. The 2H mode has a similar double peak density profile with the FH mode, but with the maximums located at $\theta = \pm\pi/2$ (compared to Figs. 2(b) and 3(b)). The density profile of 2HB mode is similar to that of 2H mode, but with two unequal peaks. The AnS mode has a similar density profile with the 2H mode but its real part exhibits an anti-symmetric shape (compared to Figs. 3(a) and 4(a)). The FHB mode has a single peak located at either $\theta = +\pi$ or $\theta = -\pi$. It should be noted that although the profile of FHB and 2HB modes seem to be asymmetric, they are actually symmetric modes by taking the periodic character of the potential into consideration. Actually, all the five types of modes can be regarded as symmetric with respect to $\theta = \pi/4$.

The stabilities of these modes are investigated via numerical computations of eigenvalues for infinitesimal perturbation modes:

$$\psi = \mathrm{e}^{-\mathrm{i}\mu z}[\phi(\theta) + \tilde{u}(\theta)\mathrm{e}^{\lambda z} + \tilde{w}^*(\theta)\mathrm{e}^{\lambda^* z}], \tag{5}$$

where $|\tilde{u}|, |\tilde{w}| \ll |\phi|$. After substitution into Eq. (1) and linearizing, we arrive at the eigenvalue problem:

$$\mathrm{i}\mathcal{L}\begin{pmatrix}\tilde{u}\\ \tilde{w}\end{pmatrix} = \lambda\begin{pmatrix}\tilde{u}\\ \tilde{w}\end{pmatrix}, \tag{6}$$

where

$$\mathcal{L} = \begin{pmatrix}L_{11} & L_{12}\\ L_{21} & L_{22}\end{pmatrix},$$

$$L_{11} = \mu + (1/2)\partial_{\theta\theta} - V(\theta) + 2\sigma|\phi|^2 - \mathrm{i}\omega\frac{\partial}{\partial\theta},$$

$$L_{12} = \sigma u^2, \quad L_{21} = -\sigma(u^2)^*,$$

$$L_{22} = -\mu - (1/2)\partial_{\theta\theta} + V(\theta)^* - 2\sigma|\phi|^2 - \mathrm{i}\omega\frac{\partial}{\partial\theta}.$$

The underlying solution ϕ is stable if all the eigenvalues are real.

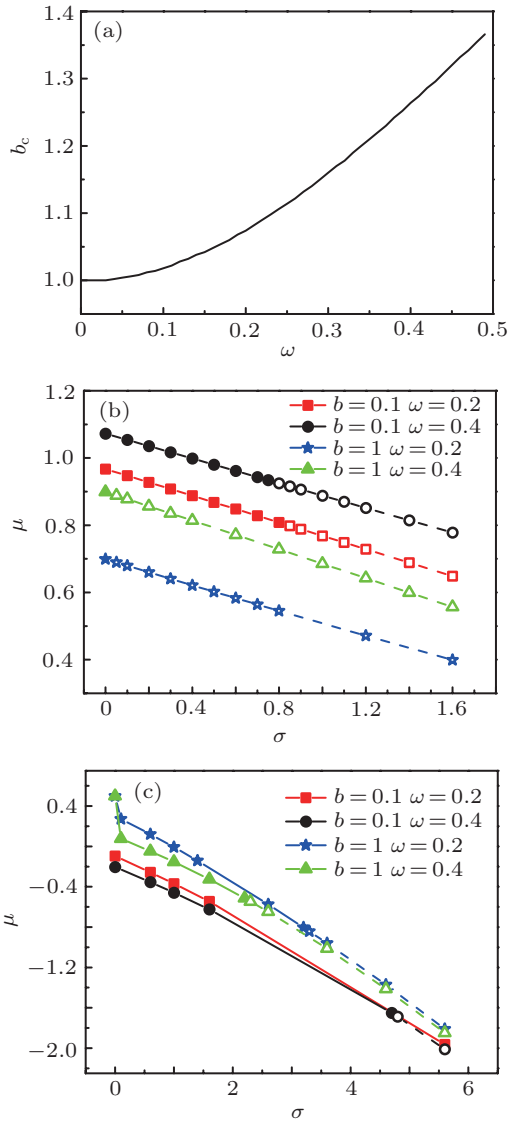


Fig. 5. (color online) (a) The critical value of b verses the rotating speed ω; (b) the bifurcation diagram in the parameter plane of μ–σ for the FH mode; (c) the bifurcation diagram for the AnS mode. In panels (b) and (c), the total power is fixed at $P = 1$, $\sigma = 0$ corresponds to the linear case. The solid symbols and lines denote the stable branches, while the hollow symbols and dashed lines denote the unstable branches. Different colors denote specific parameter settings of (b, ω), as indicated by the legends.

For the corresponding linear problem of Eq. (2), i.e., $\sigma = 0$, there exists a critical value of b above which the energy spectrum of all the linear modes will become complex. In Fig. 5(a) we plot this critical value b_c versus the rotating speed ω. It shows that b_c coincides with the strength of the real part of the $\mathcal{PT}$ potential, $a = 1$, as the system is stationary and increases with the rotating speed ω. Therefore for the nonlinear modes we investigated, the value of b is chosen to be in the interval $b = [0, 1]$. In the linear case, only three modes exist, namely the FH, 2H, and the AnS modes, and as long as b does not exceed the critical value, these three linear modes are unconditionally stable. So it is interesting to show how the families of the nonlinear modes bifurcate from the linear ones and how the nonlinearity affects the stability of these modes first. In Figs. 5(a), 5(b), and 6, the bifurcation diagrams of the five types of modes are plotted in the μ–σ plane, under different settings of (b, ω). In these figures, the total power is fixed at $P = 1$ and $\sigma = 0$ corresponds to the linear case, where only FH, 2H, and AnS modes exist. When the nonlinearity is adding on, the linear FH and AnS modes will transform continuously into the corresponding nonlinear modes and keep stable until linearity exceeds some threshold, as shown in Figs. 5(b) and 5(c). The stability of the nonlinear FH and AnS modes can be affected significantly by the value of b and ω: larger b and/or larger ω can shorten the stable branches of the nonlinear modes. This affection is more serious for the FH mode than the AnS mode, as we can see from Fig. 5(b).

The remaining three nonlinear modes, the 2H, FHB, and 2HB modes, all emerge from the linear 2H mode, as shown in Fig. 6. With the nonlinearity increasing from 0, the linear 2H mode first transforms continuously into the nonlinear 2H mode and remains stable. However, when the nonlinearity exceeds some threshold value, the nonlinear 2H mode becomes unstable and the nonlinear 2HB mode bifurcates from it at this point. If the nonlinearity increases further, the 2HB mode will transform into the FHB mode eventually. Finally, when the nonlinearity exceeds some critical value, the FHB mode will cease to exist (marked by the red cross). As for the stability, the overall character is similar to that of the FH and AnS modes, that is, larger b and ω can both make the stable beaches of 2H, FHB, and 2HB modes become shorter. However the details are more complicated as figure 6 indicated. It is interesting to note that the 2H mode regains the stability when σ is large enough, which makes the bifurcation between 2H mode and FHB mode either be supercritical (Fig. 6(a)) or be subcritical (Fig. 6(b)).

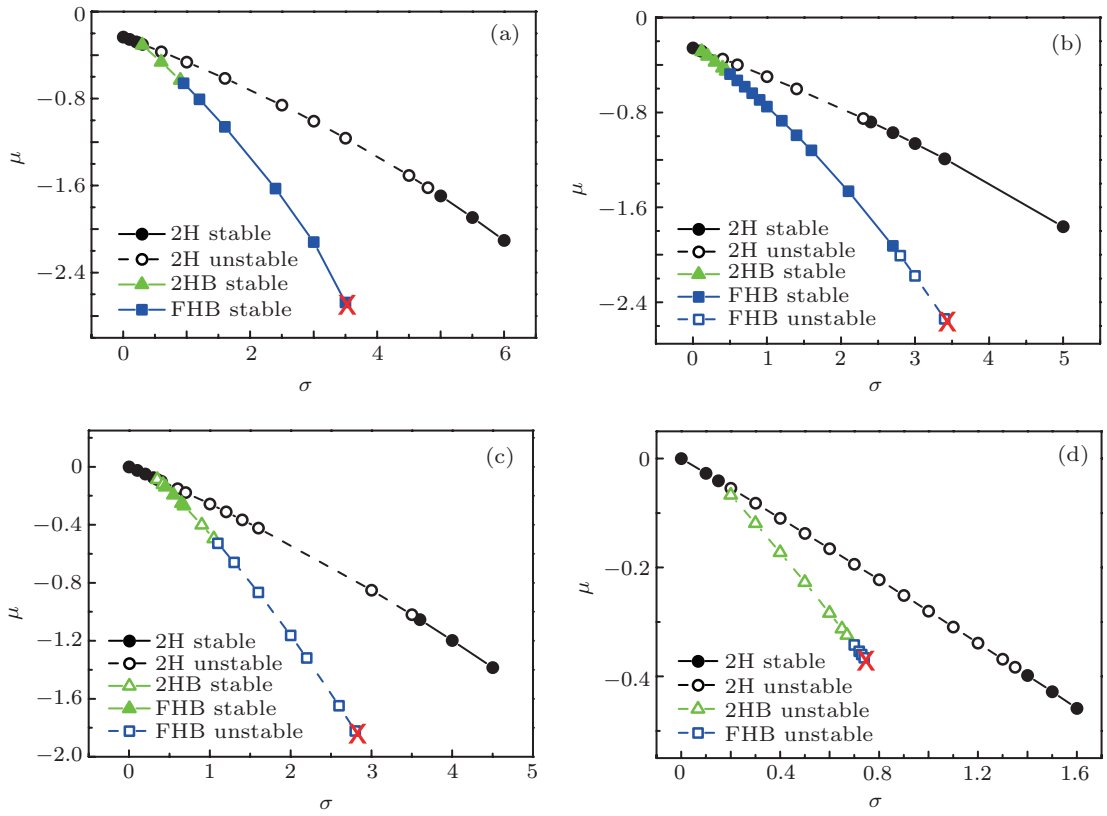


Fig. 6. (color online) The bifurcation diagram for 2H, FHB, 2HB modes in the parameter plane of μ–σ. (a) $(b, \omega) = (0.1, 0.2)$, (b) $(b, \omega) = (0.1, 0.4)$, (c) $(b, \omega) = (1, 0.2)$, and (d) $(b, \omega) = (1, 0.4)$. In all the panels, the total power of the mode is fixed at $P = 1$. The solid symbols and lines denote the stable branches, while the hollow symbols and dashed lines denote the unstable branches. Colors black, blue, and green distinguish the 2H, 2HB, and FHB modes respectively. The red cross marks the end of the branch.

To show the stability properties of these nonlinear modes more clearly, stable area diagram are plotted in the P–ω plane in Figs. 7 and 8. In these figures the nonlinearity is chosen to be $\sigma = 0.5$. From Fig. 7 we can see that there is no overlap between the stable regions of the 2H, 2HB, and FHB modes. When b increases from $b = 0.1$ to $b = 0.5$, the stable region of these three modes expands slightly. On the contrary, the stable area of the FH mode overlaps with 2H, 2HB, and FHB modes, which means in specific parameter regions the FH mode and 2H (or 2HB or FHB) mode can both stably exist. What is more, with b increasing, the stable area of FH mode shrinks significantly (compared with Figs. 7(a) and 7(a)). This is in agreement with the results presented in Fig. 5(b) that the FH mode is more subtle to the value of b. The reason may lie in the fact that the FH mode's profile is wider than that of the other modes. Compared Fig. 2(a) with Figs. 2(d), 3(b), 3(d), and 4(b), we can see that the peak of the FH mode occupies an interval of π ($[-\pi/2, \pi/2]$) in the θ axis, while the peak of the other modes occupies only a $\pi/2$ interval.

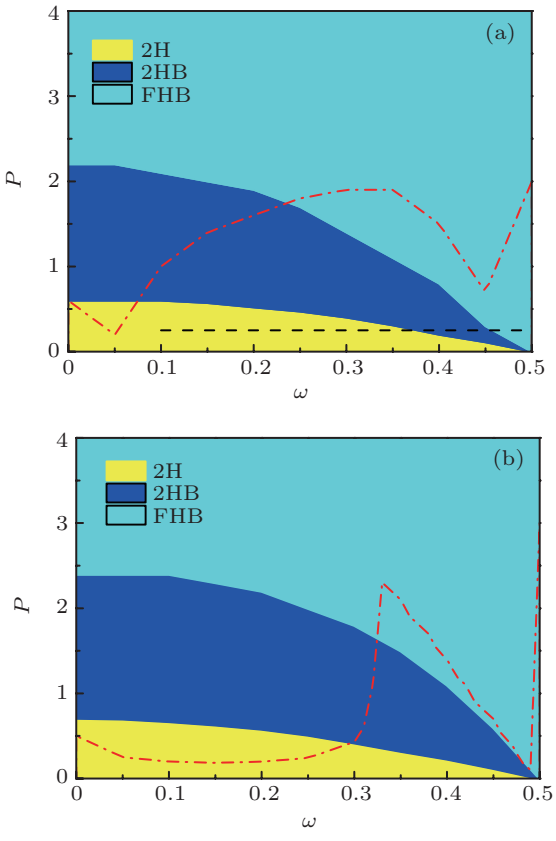


Fig. 7. (color online) Stability diagrams for FH, FHB, 2H, and 2HB modes in the SF nonlinearity, in the plane of the rotating speed ω and the total power P, at different values of the $\mathcal{PT}$'s strength: (a) $b = 0.1$, (b) $b = 0.5$. The yellow (bottom), blue (middle), and cyan (top) areas are where the 2H, 2HB, and FHB modes exist stably respectively. The area under the dash–dot line is the stable region of the FH mode. The chemical potential along the dashed line in panel (a) is calculated and shown in Fig. 9.

The wider profile makes the FH mode have more overlaps with the $\mathcal{PT}$ potential, compared to the other modes, and this may cause the subtle stability of FH mode when b is varying. The stable diagrams of the AnS mode are shown in Fig. 8. It shows that the stable area of AnS mode contracts slowly with the increasing of b. Comparing Fig. 8 with Fig. 7, it can be seen that the stable area of AnS mode overlaps with the other modes, thus in the overlap areas of Fig. 7 there actually stably exist three modes, the FH mode, 2H (or 2HB or FHB) mode, and the AnS mode. Additionally, when $b = 0$ the situation will return to the case without $\mathcal{PT}$ potential.[36]

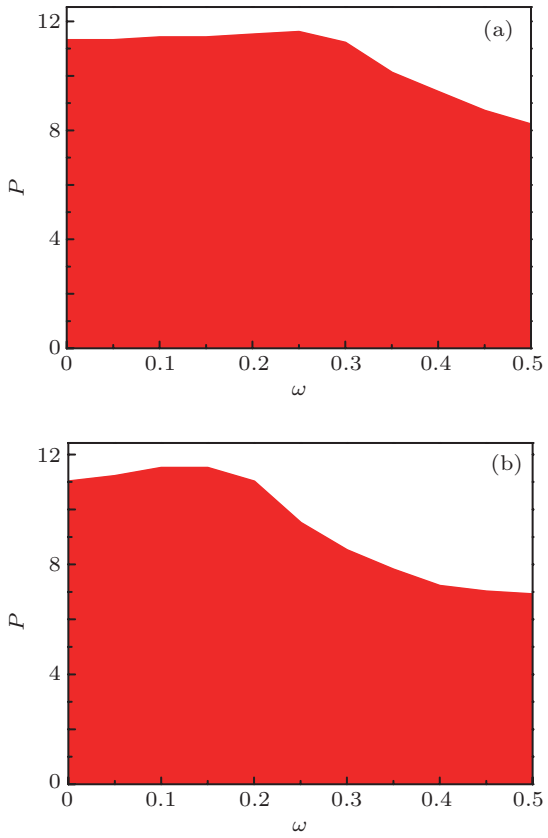


Fig. 8. (color online) Stability diagrams for AnS mode in the SF nonlinearity, in the plane of the rotating speed ω and the total power P, at different values of the $\mathcal{PT}$'s strength: (a) $b = 0.1$, (b) $b = 0.5$.

The overlaps between the stable area of these modes make it necessary to compare the energies, i.e., the chemical potential defined in Eq. (2). The results are depicted in Fig. 9. It shows that although the FH and AnS modes can stably exist with the other three types of modes, the energy of the FH mode always surpasses that of the other modes. Among the rest of the four types of modes, AnS mode always has a greater energy than the 2H, 2HB, and FHB modes. Thus the 2H or 2HB or FHB mode will become the real ground mode given specific parameter settings. Thus we have the relation between the energy of different modes as follows:

$$\mu_{2H} \quad \text{or} \quad \mu_{2HB} \quad \text{or} \quad \mu_{FHB} < \mu_{AnS} < \mu_{FH}. \tag{7}$$

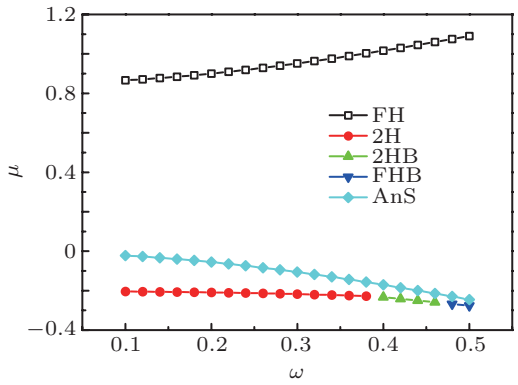


Fig. 9. (color online) The chemical potential μ calculated along the dashed horizontal line in Fig. 7(a) with $b = 0.1$, $P = 0.25$.

In Fig. 10 we plot the transverse power flow density, which is defined as $S = (\mathrm{i}/2)(\phi\phi^*_\theta - \phi^*\phi_\theta)$, versus the rotating speed ω for FH, FHB, 2H, 2HB, and AnS modes. We can see from this figure that the rotating has different effects on the behavior of the power flow for each mode. For FHB (Fig. 10(b)) and AnS (Fig. 10(e)) modes the power flow is always positive, indicating that the power always flows from gain to loss region, and S increases with ω increasing. For 2H (Fig. 10(c)) and 2HB (Fig. 10(d)) modes, the direction of the flow varies across the potential, and the absolute value of the flow also increases with ω increasing. For FH mode, however, figure 10(a) shows that when the potential is stationary ($\omega = 0$) the power flow is always positive, but with ω increasing, the direction of the flow changes steeply and when $\omega > 0.1$ the flow becomes negative across the whole potential, which indicates a sudden inverse of the power flow direction.

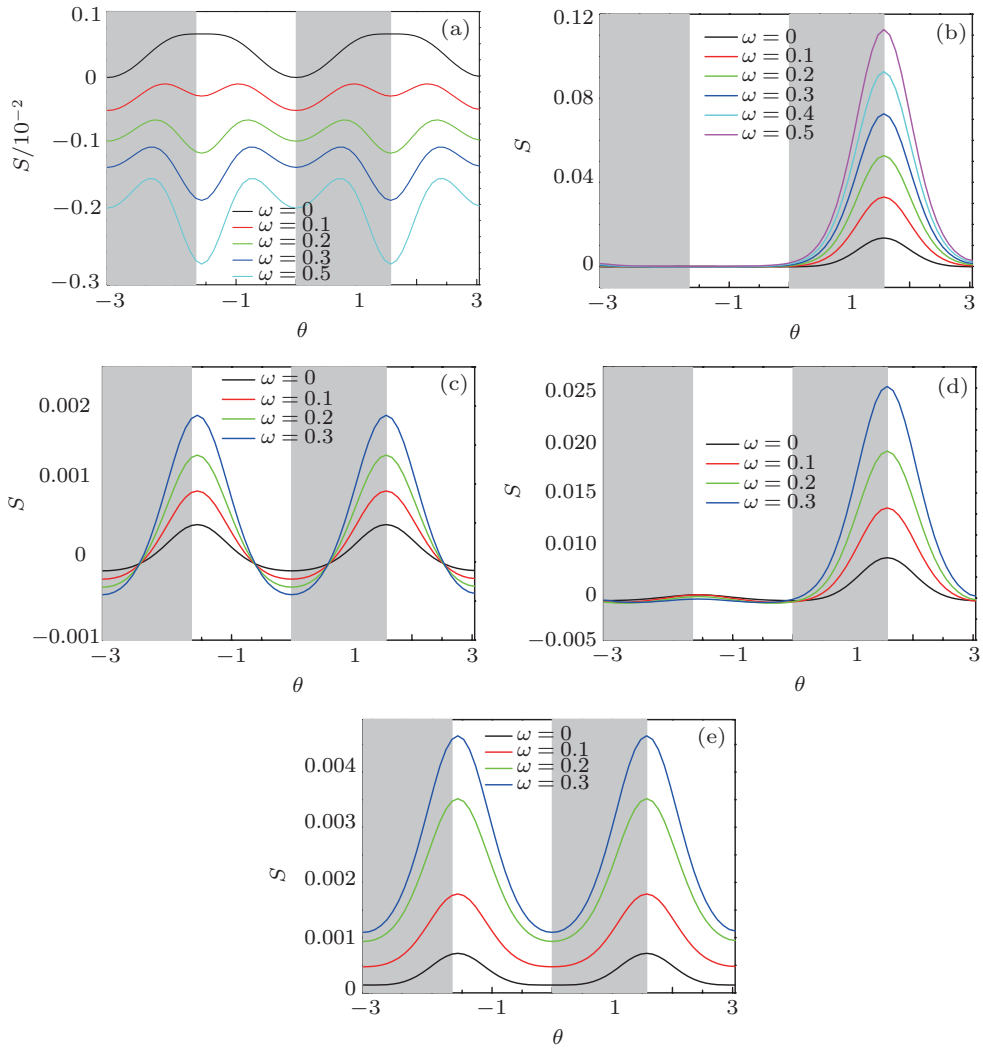


Fig. 10. (color online) The transverse power flow density S versus rotating speed ω under $b = 0.1$: (a) FH mode with $P = 0.2$; (b) FHB mode with $P = 2.5$; (c) 2H mode with $P = 0.2$; (d) 2HB mode with $P = 1.0$; (e) AnS mode with $P = 0.2$. The gray (white) area depicts the loss (gain) region of the potential.

4. Conclusions

In conclusion, we studied the nonlinear modes in a rotating double-well potential with $\mathcal{PT}$ symmetry. We found that stable nonlinear mode can exist in this dynamical system driven by a rotation. The five types of stable modes, namely FH, FHB, 2H, 2HB, and AnS modes, are identified in this sys-

tem. The bifurcation of these nonlinear modes from the corresponding linear modes are studied. The results show that the nonlinear FH, AnS, and 2H modes continue from the linear FH, 2H, and AnS modes respectively, while the 2HB and FHB modes bifurcate from the nonlinear 2H mode with the nonlinearity increasing. A larger nonlinearity and/or a faster rotation can make the stable branches of these nonlinear modes become shorter. The stability properties of these soliton modes are investigated and the stable diagrams for each mode in the P–ω plane are presented. Results show that there is no overlapping stable area between FHB, 2HB, and 2H modes, but the FH and AnS modes can coexist with the other three types of modes in certain parameter region. Increasing the strength of the imaginary part of the $\mathcal{PT}$ potential will change the shape of the stable area of the FH mode significantly. The chemical potential of these modes shows that the FHB, 2H or 2HB modes are the real ground mode of the system. The effects of the rotation on the modes are studied, for the FH mode, an inversion of the transverse power flow density is found, thus when the rotating speed ω exceeds a threshold value, the power flow will invert its direction.

References

[1] Bender C M 2007 *Rep. Prog. Phys.* **70** 947
[2] Bender C M and Boettcher S 1998 *Phys. Rev. Lett.* **80** 5243
[3] Ruschhaupt A, Delgado F and Muga J G 2005 *J. Phys. A: Math. Gen.* **38** L171
[4] Guo A, Salamo G J, Duchesne D, Morandotti R, Volatier-Ravat M, Aimez V, Siviloglou G A and Christodoulides D N 2009 *Phys. Rev. Lett.* **103** 093902
[5] Rüter C E, Makris K G, El-Ganainy R, Christodoulides D N, Segev M and Kip D 2010 *Nat. Phys.* **6** 192
[6] Regensburger A, Bersch C, Miri M A, Onishchukov G, Christodoulides D N and Peschel U 2012 *Nature* **488** 167
[7] Bender N, Factor S, Bodyfelt J D, Ramezani H, Christodoulides D N, Ellis F M and Kottos T 2013 *Phys. Rev. Lett.* **110** 234101
[8] Klaiman S, Günther U and Moiseyev N 2008 *Phys. Rev. Lett.* **101** 080402
[9] Schindler J, Li A, Zheng M C, Ellis F M and Kottos T 2011 *Phys. Rev. A* **84** 040101
[10] Bittner S, Dietz B, Günther U, Harney H L, Miski Oglu M, Richter A and Schäfer F 2012 *Phys. Rev. Lett.* **108** 024101
[11] Li K and Kevrekidis P G 2011 *Phys. Rev. E* **83** 066608
[12] Zezyulin D A and Konotop V V 2012 *Phys. Rev. Lett.* **108** 213906
[13] He Y and Mihalache D 2012 *Rom. Rep. Phys.* **64** 1243
[14] Akhmediev N and Ankiewicz A 2005 *Dissipative Solitons* (Berlin: Springer)
[15] Zhou K, Guo Z, Wang J and Liu S 2010 *Opt. Lett.* **35** 2928
[16] Wang H and Wang J 2011 *Opt. Express* **19** 4030
[17] Lu Z and Zhang Z M 2011 *Opt. Express* **19** 11457
[18] Abdullaev F K, Kartashov Y V, Konotop V V and Zezyulin D A 2011 *Phys. Rev. A* **83** 041805
[19] Zezyulin D A, Kartashov Y V and Konotop V V 2011 *Europhys. Lett.* **96** 64003
[20] He Y, Zhu X, Mihalache D, Liu J and Chen Z 2012 *Phys. Rev. A* **85** 013831
[21] Huang C, Li C and Dong L 2013 *Opt. Express* **21** 3917
[22] Hu S M and Hu W 2012 *Chin. Phys. B* **21** 024212
[23] Hu S M, Lu D Q, Ma X K, Guo Q and Hu W 2012 *Europhys. Lett.* **98** 14006
[24] Li C Y, Huang C M, Liu H D and Dong L W 2012 *Opt. Lett.* **37** 4543
[25] Hu S M and Hu W 2013 *Chin. Phys. B* **22** 074201
[26] Konotop V V, Pelinovsky D E and Zezyulin D A 2012 *Europhys. Lett.* **100** 56006
[27] Li C Y, Huang C M and Dong L W 2013 *Chin. Phys. B* **22** 074209
[28] Fetter A E 2009 *Rev. Mod. Phys.* **81** 647
[29] Engels P, Coddington I, Haljan P C, Schweikhard V and Cornell E A 2003 *Phys. Rev. Lett.* **90** 170405
[30] Sakaguchi H and Malomed B A 2008 *Phys. Rev. A* **78** 063606
[31] Tung S, Schweikhard V and Cornell E A 2006 *Phys. Rev. Lett.* **97** 240402
[32] Kakarantzas G, Blanch A O, Birks T A, Russell P St J, Farr L, Couny F and Mangan B J 2003 *Opt. Lett.* **28** 158
[33] Kartashov Y V, Malomed B A and Torner L 2007 *Phys. Rev. A* **75** 061602
[34] Sakaguchi H and Malomed B A 2007 *Phys. Rev. A* **75** 013609
[35] Sakaguchi H and Malomed B A 2009 *Phys. Rev. A* **79** 043606
[36] Li Y Y, Pang W and Malomed B A 2012 *Phys. Rev. A* **86** 023832
[37] Lederer F, Stegeman G I, Christodoulides D N, Assanto G, Segev M and Silberberg Y 2008 *Phys. Rep.* **463** 1
[38] Li Y Y, Malomed B A, Feng M and Zhou J 2010 *Phys. Rev. A* **82** 063813
[39] Pang W, Wu J, Yuan Z, Liu Y and Chen G 2011 *J. Phys. Soc. Jpn.* **80** 113401
[40] Wu J, Feng M, Pang W, Fu S and Li Y 2011 *J. Nonlinear Opt. Phys.* **20** 193
[41] Li H J, Dou J P, Yang J J and Huang G X 2013 *Opt. Express* **21** 32053
[42] Smyrnakis J, Bargi S, Kavoulakis G M, Magiropoulos M, Karkkäinen K and Reimann S M 2009 *Phys. Rev. Lett.* **103** 100404
[43] Hang C, Huang G X and Konotop V V 2013 *Phys. Rev. Lett.* **110** 083604
[44] Saito H and Ueda M 2004 *Phys. Rev. Lett.* **93** 220402
[45] Schwartz S, Cozzini M, Menotti C, Carusotto I, Bouyer P and Stringari S 2006 *New J. Phys.* **8** 162
[46] Carretero-González R, Frantzeskakis D J and Kevrekidis P G 2008 *Nonlinearity* **21** R139
[47] Yang J and Lakoba T I 2007 *Stud. Appl. Math.* **118** 153